Spotlight-mode Synthetic Aperture Radar Processing for High-Resolution Lunar Mapping

Leif Harcke*, Lawrence Weintraub†, Sang-Ho Yun*, Richard Dickinson†,
Eric Gurrola*, Scott Hensley*, and Nicholas Marechal†
*Jet Propulsion Laboratory, 4800 Oak Grove Dr., Pasadena, CA 91109
Phone: 1-818-354-0281 Email: leif.j.harcke@jpl.nasa.gov
†The Aerospace Corporation, 2310 E. El Segundo Blvd., El Segundo, CA 90245

***Abstract*— During the 2008–2009 year, the Goldstone Solar System Radar was upgraded to support radar mapping of the lunar poles at 4 m resolution. The finer resolution of the new system and the accompanying migration through resolution cells called for spotlight, rather than delay-Doppler, imaging techniques. A new pre-processing system supports fast-time Doppler removal and motion compensation to a point. Two spotlight imaging techniques which compensate for phase errors due to i) out of focus-plane motion of the radar and ii) local topography, have been implemented and tested. One is based on the polar format algorithm followed by a unique autofocus technique, the other is a full bistatic time-domain backprojection technique. The processing system yields imagery of the specified resolution. Products enabled by this new system include topographic mapping through radar interferometry, and change detection techniques (amplitude and coherent change) for geolocation of the NASA LCROSS mission impact site.**

I. Introduction

As described in a companion paper [1], during the 2008–2009 year, the Goldstone Solar System Radar was upgraded to support radar mapping of the lunar poles at 4 m resolution. The hardware modifications consisted of a commercial digital waveform generator modulating a 40 MHz bandwidth chirp, and a commercial digitizer and FPGA processor implementing digital downconversion of the radar's IF band. Parameters of the new acquisition system are listed in Table I.

The capability of the new hardware, which increased the range bandwidth from 10 MHz to 40 MHz and changed the pulse modulation from maximal-length PN sequences to a linear FM chirp, required the development of a new signal processing and imaging system to support 4 m resolution mapping. In previous lunar mapping experiments, the radar hardware corrected for instantaneous or "fast time" Doppler on transmit via ephemeris steering of the transmitter local oscillator and timebase drifting of the PN code generator clock and receiver sample clocks. Range compression was applied in non-real time by correlating with the ideal transmitted PN sequence, and unfocused delay-Doppler or focused range-Doppler imaging algorithms were employed [2], [3], [4].

In the new Goldstone configuration, the transmit local oscillator and all sample clocks are fixed. Fast-time Doppler removal and data resampling must be performed in non-real time by the data processing system. In addition, the finer resolution of the new system and the accompanying migration through resolution cells called for spotlight, rather than delay-Doppler imaging techniques [5].

TABLE I
Radar System Parameters

Parameter	Value
Radar band	X-band
Carrier frequency	8560 MHz
Pulse bandwidth	40 MHz
Pulse modulation	Linear FM chirp
Range resolution	4 m
Standoff range	370,000 km
Pulse duration	12.5 or 20 millisec
Pulse repetition frequency	50 or 80 Hz
IF frequency	460 MHz
IF bandwidth	50 MHz
Digitizer bit depth	8 bits
Sampling frequency	1280 Msps real
Baseband recording rate	80 Msps complex
Synthetic aperture time	90 min.
Synthetic aperture length	2,300 km
Cross-range resolution	5 m
Area coverage	430,000 km^2
Data volume	1,600 Gbyte

II. Ephemeris and Coordinate Systems

The fundamental ephemeris for the Moon's center of mass is the JPL developmental ephemeris DE-421 [6]. DE-421 also defines the Mean Earth or ME lunar reference orientation frame. A Cartesian coordinate system for lunar mapping, known as the unified lunar control network ULCN 2005, has been specified by the U.S. Geological Survey and based on optical imagery photogrammetry from the Clementine mission [7]. State vectors for the apparent positions of the transmitting and receiving deep space network antennas were extracted from the fundamental ephemeris by two independent software systems, an internal JPL system and the widely available SPICE system [8]. Cross-checking of the two products verified proper formulation of light time corrected state vectors and predicted Doppler frequencies.

Though the DE-421 base product is integrated in quad precision floating point, the end-user software systems employ double-precision floating point only. For the 3.5 cm wavelength of the radar at standoff ranges of several hundred thousand kilometers, the numerical noise in representing time

and positions causes unwanted phase noise or increased multiplicative noise ratio (MNR) in the final imagery products. To mitigate these issues, polynomial smoothing is applied to the output state vectors.

III. Range Compression

The transmitter emits linear FM pulses at a constant pulse repetition rate. Since the round-trip travel time to the Moon changes with time, the received signal is a distorted version of the transmitted chirp. For example, if we time tag the beginning of each chirp at a rate of 12.5 msec on the transmit side, the associated receive time tags are not evenly distributed. Conversely, if we time tag the received signal at a constant rate, the associated transmit time tags are not at constant rate. Since the propagation delay of several seconds is quite long compared to the pulse interval, careful accounting of time is required to match the received pulse records with the ephemeris.

A. Fast-time Doppler Removal

A set of time tags are defined as follows:

$$\begin{aligned} t^T_{tx}(n) &: \text{ Transmit based transmit time tag array} \\ t^T_{rx}(n) &: \text{ Transmit based receive time tag array} \\ t^R_{tx}(n) &: \text{ Receive based transmit time tag array} \\ t^R_{rx}(n) &: \text{ Receive based receive time tag array} \end{aligned}$$

The subscript $_{tx}$ and $_{rx}$ mean that the quantity is at transmitter and receiver respectively, and the superscript ^{T} and ^{R} mean that the time tags are based on, or specified at, the transmitter and receiver respectively. If the subscript and the superscript match, the quantity is specified (i.e. independent variable). If they do not match, the quantity is calculated based the time tags on the superscript's station (i.e. dependent variable). Note that if $t^T_{tx}(n)$ and $t^R_{rx}(n)$ have constant intervals, then their pairs, $t^T_{rx}(n)$ and $t^R_{tx}(n)$, do not have constant intervals. The time tags used in the range compression process are $t^T_{tx}(n)$, $t^T_{rx}(n)$, and $t^R_{rx}(n)$. $t^T_{tx}(n)$ are at the start time of each transmitted chirp, thus $t^T_{tx}(n+1)-t^T_{tx}(n) = 12.5$ msec. $t^T_{rx}(n)$ are receive time tags of radar signal that were transmitted at $t^T_{tx}(n)$. Finally, $t^R_{rx}(n)$ are the nearest data sample to $t^T_{rx}(n)$. Also note that the first two and the last two are related as follows:

$$\begin{aligned} t^T_{rx}(n) &= t^T_{tx}(n) + \Delta t^T(n) \\ t^R_{tx}(n) &= t^R_{rx}(n) - \Delta t^R(n) \end{aligned} \tag{1}$$

where $\Delta t^T(n)$ is the round trip time of a chirp that is transmitted at time $t^T_{tx}(n)$, and $\Delta t^R(n)$ is the round trip time of a chirp that is received at time $t^R_{rx}(n)$. These two quantities are estimated from Chebyshev polynomials, whose coefficients are given in the ephemeris files.

In order to derive the effect of the round trip time on the received signal and its relationship to Doppler frequency, let us consider continuous time t_{tx} and t_{rx}. They are related to each other as

$$t^T_{rx} = t^T_{tx} + \Delta t^T(t_{tx}) \tag{2}$$

$$t^R_{tx} = t^R_{rx} - \Delta t^R(t_{rx}) \tag{3}$$

for transmit based and receive based respectively. Here transmit based means that the time t^T_{tx} is marching at a constant rate, but t^T_{rx} is not, due to the time varying $\Delta t^T(t_{tx})$. Receive based means that the time t^R_{rx} is marching at a constant rate, but t^R_{tx} is not.

The basic concept and notations are adapted from prior JPL work. For a waveform, $m(t)$, modulating a radio frequency carrier at f_c the transmitted signal is

$$x_t(t_{tx}) = m(t_{tx})\, e^{i(2\pi f_c t_{tx} + \phi_o)}$$

where ϕ_o is a constant, but unknown, phase offset. Then let $x_r(t_{rx})$ be a point target response, the received signal bounced at an ideal point target located at the antenna's aim point on the moon. Because the received signal x_r at time t_{rx} is the transmitted signal x_t at time t_{tx}, either transmit based or receive based,

$$\begin{aligned} x_r(t^R_{rx}) &= x_t(t^R_{tx}) && (4) \\ &= m(t^R_{tx})\, e^{i(2\pi f_c t^R_{tx} + \phi_o)} && (5) \\ &= m(t^R_{tx})\, e^{i(2\pi f_c (t^R_{rx} - \Delta t^R(t_{rx})) + \phi_o)} && (6) \\ &= m(t^R_{tx})\, e^{i2\pi f_c t^R_{rx}}\, e^{-i2\pi f_c \Delta t^R(t_{rx})}\, e^{i\phi_o}. && (7) \end{aligned}$$

Then the received signal is basebanded to remove the carrier frequency.

B. Data Interpolation and Matched Filtering

After the Doppler frequency is removed, the data can be considered a baseband chirp signal. This signal is matched-filtered with the reference chirp. Because of the time drift, however, care must be taken to ensure that the time tags of the received signal and the reference chirp are matched.

This can be done in two different ways. First, the receive based approach can be used to calculate the transmit time tags, $t^R_{tx}(n)$, and retrieve chirp samples at these time tags. That is, the transmitted chirp is resampled to match the received chirp. This approach has an advantage that the resampling process does not involve interpolation, because samples of the reference chirp can be generated from an analytical function. The reference chirp is in effect "customized" to the expected echo from a single resolution cell on the moon, but this customized warping of the chirp may not match very well the responses from other resolution cells in the radar footprint.

Alternatively, a transmit based approach can be used to calculate the expected arrival time (i.e. t^T_{rx}) of the pulse. Here, the received data must be interpolated to match a single baseband reference chirp. This approach has an advantage of keeping the transmitted chirp unchanged throughout the whole image. However, resampling the data involves expensive calculations.

Through examination of both approaches with real data sets, it was found that the transmit based approach produces images

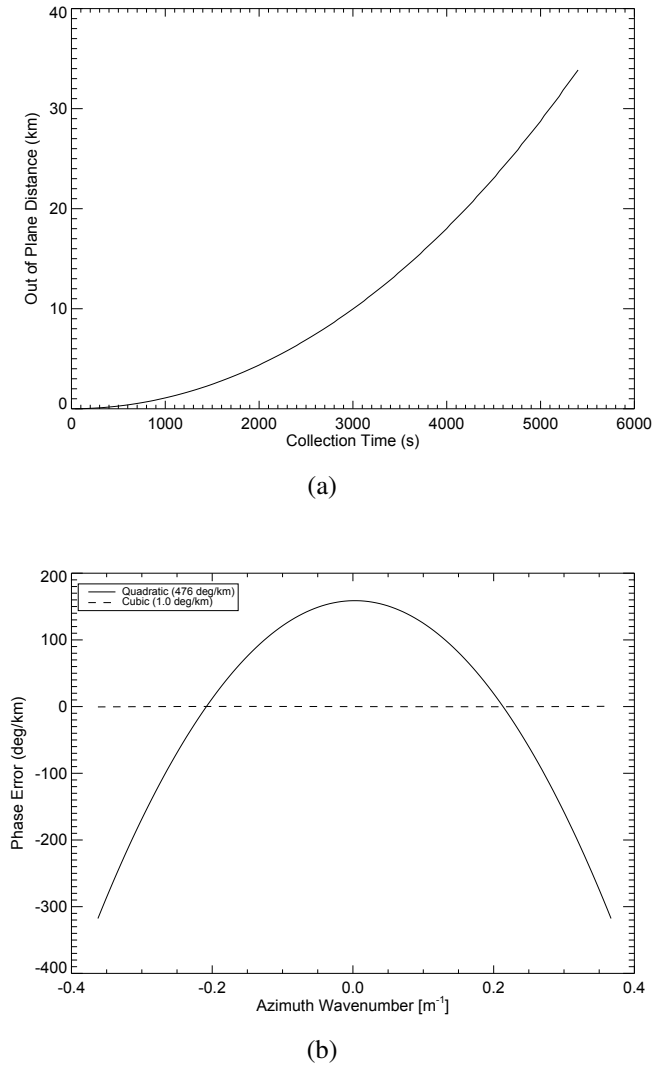

Fig. 1. Predicted out of plane motion, showing the maximum deviation from planar motion as a function of collection time (a) and phase errors for a collection of 45 minutes (b) for the lunar imaging geometry. The quadratic surface depicts out-of-plane motion, where range wavenumber is proportional to radio frequency and azimuth wavenumber is proportional to pulse index.

of better quality than the receive based approach does. While applying this transmit based approach, we used frequency-domain sinc interpolation based on the Fourier shift theorem, to avoid expensive time-domain interpolation. Time domain shift t_{shift} of fractional sample values can be accommodated by multiplying a phase ramp in frequency domain as shown in the following Fourier transform pair [9]

$$g(t - t_{\text{shift}}) \quad \supset \quad G(f)\, e^{-i2\pi f t_{\text{shift}}}. \tag{8}$$

Here $G(f)$ is the Fourier transform of $g(t)$. The shift is uniformly applied to each pulse record.

IV. Spotlight-mode Imaging

The standoff range and fine resolution of the system place stringent requirements on the accuracy of the synthetic aperture focusing function. Sources of phase error and defocus include: i) relative motion knowledge errors between the radar antennas on the surface of the Earth and the ground reference point on the lunar surface, and ii) terrain elevation variation, due to motion of antenna phase centers out of the slant-plane. Two spotlight-mode synthetic aperture imaging algorithms have been applied to the data.

A. Polar Format and Autofocus

The first approach follows the standard polar format algorithm from the literature [10], [11], with a 35 dB Taylow window for sidelobe suppression, followed by a unique autofocus algorithm. Out of slant-plane motion analysis was applied to the lunar ephemeris data for a 45 minute aperture. The out of plane correction allows scatterers in a single arbitrary focal plane to be brought in focus. All scatters outside the focal plane will suffer from a predictable, but unavoidable phase error proportional to their distance from the focal plane. The focal plane is chosen to be the plane tangent to the nominal Lunar sphere with its origin at the aim point. The choice of focal plane, and aim point, can be adjusted to any desired position and orientation during the polar format processing. Figure 1 depicts the effect of the motion. The quadratic shape is primarily a function of azimuth wavenumber, with a (not shown) much smaller secondary dependence on range wavenumber, or RF frequency. For a 45 minute collection of the Lunar South Pole, the model predicts 0.476 degrees of quadratic phase per meter or equivalently 476 degrees of quadratic for each km of scatterer displacement from the focal plane. This error scales quadratically with the resolution of the image.

Since the out of slant-plane motion could be predicted by the ephemeris, re-sampling of the data in the range-dispersed domain removed a bulk phase error component. However, correcting phase errors due to the topographic deviation from the image focus plane, which can be ± 6 km at the South Pole, requires autofocus techniques. The autofocus routines developed have both quadratic (parametric) and nonparametric phase gradient class estimators. The algorithm partitions the image into a grid of sub images and focuses each sub image, as shown in Figure 2.

B. Time-domain Backprojection

As a second type of image formation, the standard time-domain backprojection algorithm from the literature was employed [12], [13]. All pulse time delays were converted into distances in the Mean-Earth Cartesian XYZ frame, and backprojection took place in this frame. Due to the separations of the transmitting and receiving antennas, full bistatic backprojection, rather than the monostatic approximation, was employed.

Since the backprojection algorithm is order N^3, considerable speedup was achieved by programming the algorithm to run on a multi-core shared memory computer with the OpenMP parallel programming standard [14]. As a selectable parameter, a Hamming window was applied across the synthetic aperture to reduce cross-range sidelobes. To compensate

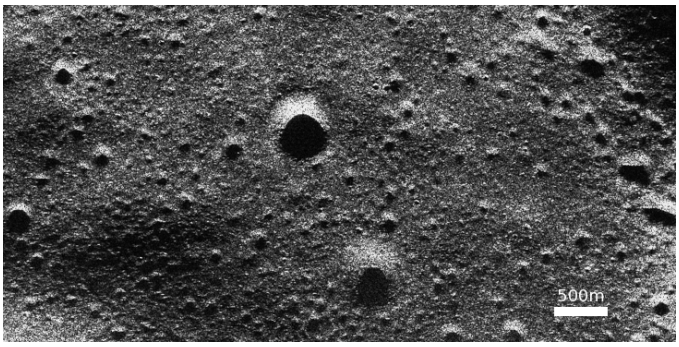

Fig. 2. Radar image near the Moon's south pole, processed to 8.7 m azimuthal resolution via the polar format algorithm followed by autofocus.

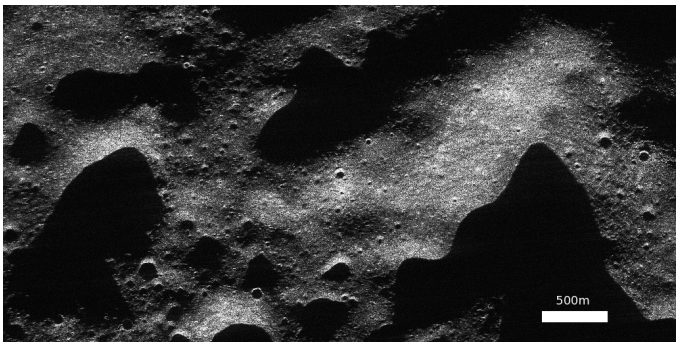

Fig. 3. Radar image of an area near the Moon's north pole, processed to 5 m resolution via the time-domain backprojection algorithm.

for topographic height variations from an ideal reference surface, the backprojection employed a 250 m resolution digital elevation model of the moon from the laser altimeter on the Japan Aerospace Exploration Agency Kaguya/SELENE mission [15]. An example of the resulting imagery is shown in Figure 3. Applying standard two-element interferometry [16], topographic height information is extracted from the data as shown in Figure 4.

V. Summary

The upgraded data processing and imaging systems for the Goldstone solar system radar are supporting 4 m imaging of the lunar surface. Future products enabled by this new system include topographic mapping through radar interferometry, and change detection techniques (amplitude and coherent change) for geolocation of the NASA LCROSS mission impact site.

VI. Acknowledgement

This work was performed under NASA contract NAS7-03001 task order NMO0711046. The Jet Propulsion Laboratory is operated by the California Institute of Technology under contract with the National Aeronautics and Space Administration.

The authors would also like to thank The Aerospace Corporation for supporting this work through its Independent Research and Development program.

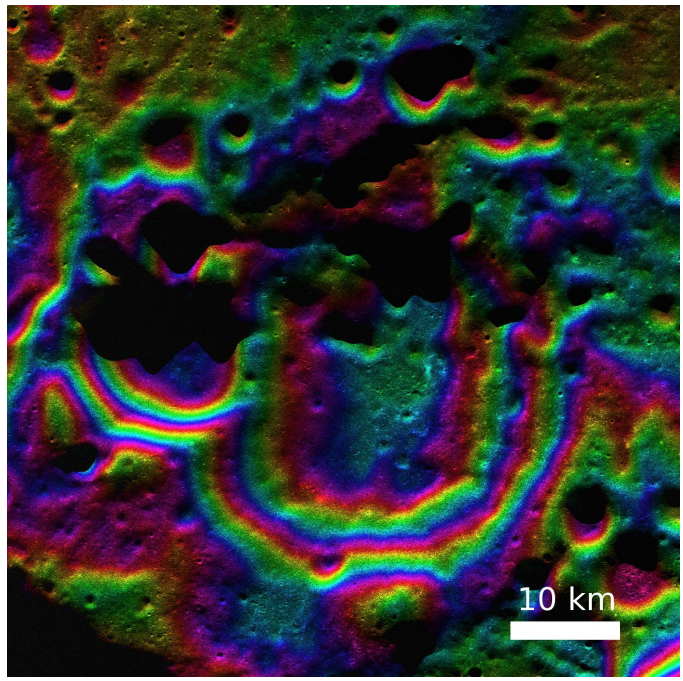

Fig. 4. Radar interferogram of the floor of Cabeus A crater in the south polar region.

References

[1] S. Hensley *et al.*, "Lunar topographic mapping using a new high resolution mode for the GSSR radar", *Proc. 2010 IEEE Radar Conf.*, Washington D.C., May 10–14, 2010.

[2] N.J.S. Stacy, *High-Resolution Synthetic Aperture Radar Observations of the Moon*, Ph.D. Thesis, Cornell University, 1993.

[3] J.L. Margot, *Lunar Topography from Earth-based Radar Interferometric Mapping*, Ph.D. Thesis, Cornell University, 1999.

[4] S. Hensley *et al.*, "An improved map of the lunar south pole with Earth-based radar interferometry," *Proc. 2008 IEEE Radar Conf.*, Rome, Italy, May 26–30, 2008, DOI 10.1109/RADAR.2008.4721077.

[5] J.L.H. Webb, D.C. Munson, and N.J.S. Stacy, "High-resolution planetary imaging via spotlight-mode synthetic aperture radar," *IEEE Trans. Image Proc.*, Vol. 7, No. 11, pp. 1571–1582, Nov. 1998.

[6] J.G. Williams, D.H. Boggs, and W.M. Folkner, "DE-421 Lunar orbit, physical librations, and surface coordinates," Interoffice memorandum No. 335-JW/DB/WF-20080314-001, Jet Propulsion Laboratory, Pasadena, CA, Mar. 14, 2008. URL: ftp://ssd.jpl.nasa.gov/pub/eph/planets/ioms/de421_moon_coord_iom.pdf

[7] B.A. Archinal, M.R. Rosiek, R.L. Kirk, and B.L. Redding, "The Unified Lunar Control Network 2005," U.S. Geological Survey, Open File Report 2006-1367, Flagstaff, AZ, 2006.

[8] C.H. Acton, "Ancillary data services of NASA's Navigation and Ancillary Information Facility," *Planetary and Space Science*, Vol. 44, No. 1, pp. 65-70, 1996.

[9] R. Bracewell, *The Fourier Transofrm and Its Applications*, McGraw-Hill, 2000.

[10] D.E. Wahl, P.H. Eichel, D.C. Ghiglia, P.A. Thompson, and C.V. Jakowatz, *Spotlight-mode Synthetic Aperture Radar*, Springer, 1996.

[11] W.G. Carrara, R.S. Goodman, and R.M. Majewski, *Spotlight Synthetic Aperture Radar*, Artech House, 1995.

[12] M.D. Desai and W.K. Jenkins, "Convolution backprojection image reconstruction for spotlight mode synthetic aperture radar", *IEEE Trans. Image Processing*, Vol. 1, No. 4, Oct. 1992.

[13] M. Soumekh, *Synthetic Aperture Radar Signal Processing*, Wiley, 1999.

[14] R. Chandra, L. Dagum, D. Kohr, D. Maydan, J. McDonald, and R. Menon, *Parallel Programming in OpenMP*, Morgan Kaufmann, 2001.

[15] H. Araki *et al.*, "Lunar shape and polar topography derived from Kaguya-LALT laser altimetry," *Science*, Vol. 323, No. 5916, pp. 897–900m Feb. 2009.

[16] S.H. Zisk, "A new, Earth-based radar technique for the measurement of lunar topography," *Earth, Moon, and Planets*, Vol. 4, No. 3–4, pp. 296–306, Sep. 1972.